PAPER

Check for updates

Visible LED-based photo-redox properties of sulfur and nitrogen-doped carbon dots designed by solid-state synthesis†

Neha Kaushal,[ab] Amit L. Sharma[ab] and Avishek Saha*[ab]

Nitrogen-doped and sulfur, nitrogen co-doped carbon dots (CDs) were synthesized using a solid-state, solvent-free, microwave synthesis technique at 250 °C. CDs were synthesized using citric acid as the carbon precursor and urea or thiourea as the nitrogen and sulfur precursor. The solid-state synthesis produced crystalline nitrogen-doped CDs (N-CDs) and nitrogen/sulfur co-doped CDs (S,N-CDs) with a broad absorption band in the visible region. The photoredox catalytic properties of the as-prepared CDs were demonstrated by investigating the model photoreduction of methyl viologen using 410 nm and 455 nm light-emitting diodes (LEDs). The highest concentration of the methyl viologen radical cation was monitored in the presence of N-CDs in comparison with S,N-CDs. The results indicate that nitrogen-doped graphitic CDs feature higher charge extraction for photoredox catalysis in comparison to nitrogen, sulfur co-doped CDs.

Introduction

Carbon dots (CDs) have attracted significant research interest since their discovery in 2004.[1] Due to their unique properties such as high stability, tunable photoluminescence, chemical inertness, and biocompatibility, CDs have been investigated for a wide range of applications, including photocatalysis,[2–4] sensing,[5–8] electrocatalysis,[9–11] biomedical applications,[12–15] *etc.* In general, CDs consist of organic functional groups covalently attached to the core semiconducting graphitic domain featuring photoluminescence properties from the UV to near IR region of the solar spectrum. In this context, recent studies have suggested that the conventional bottom-up synthesis of carbon nanodots is likely to produce molecular side-products including citrazinic acid and 4-hydroxy-1*H*-pyrrolo[3,4-*c*]pyridine-1,3,6(2*H*,5*H*)-trione (HPPT).[16–18] Although the presence of a complex variety of photoluminescent molecules in CDs is attractive for sensing applications, these fluorescent molecules are not desirable for the photoredox catalytic process.

Thermal solid-phase synthesis could prevent the formation of these complex molecular by-products and facilitate the construction of a graphitic domain of CDs.[19,20] For example, Reisner *et al.* demonstrated that increasing the synthesis temperature will increase the graphitized carbon core.[4]

They have further reported that graphitized carbon dots exhibit better photocatalytic activity than amorphous carbon dots. In particular, the microwave-assisted solvent-free synthesis method has several advantages, including short reaction time, reproducibility, and scalability.[20] Apart from solid-state synthesis, doping of carbon nanodots with heteroatoms like nitrogen, sulfur, *etc.* could be another strategy to improve the photoredox properties of CDs. Nitrogen is the most frequently used element due to its easy doping process and comparative atomic size. Core nitrogen doping can have a consequential impact on photocatalysis by tuning the absorption towards the visible spectrum and by facilitating the light induced charge transfer process. Also, doping of carbon dots with sulphur atoms can result in the enhancement of electron donating efficiency of CDs and thus elevate the efficiency of the photo-catalytic process. To this end, N and/or S doped CDs have demonstrated enhanced photocatalytic and photoredox properties.[21,22]

To this end, very few studies are there on the photoredox properties of doped and graphitized carbon dots synthesized by solid-phase, bottom-up synthesis. Cailotto *et al.* performed comparative studies on photoinduced electron transfer from different amorphous and graphitized carbon nanodots, without introducing any heteroatoms.[22] On the other hand, Prato *et al.* investigated the photocatalytic properties of nitrogen-doped carbon dots produced by liquid phase microwave synthesis. Still, the crystalline/amorphous nature of the core of carbon dots has not been studied.[23] To enhance the photocatalytic properties of carbon dots, it is crucial to investigate the electron

a Central Scientific Instruments Organisation (CSIR-CSIO), Sector 30-C, Chandigarh-160030, India. E-mail: avishek.saha@csio.res.in
b Academy of Scientific and Innovative Research (AcSIR-CSIO), Ghaziabad-201002, India

† Electronic supplementary information (ESI) available. See DOI: 10.1039/d1ma00860a

transfer properties of different heteroatoms doped, crystalline carbon dots.

In this work, we have synthesized graphitized N-doped and S,N-doped carbon dots at 250 °C following the solid-phase microwave synthesis route. Furthermore, investigation of the photoinduced electron transfer properties has been carried out by performing the photoreduction of methyl viologen with 410 and 455 nm LED sources. This study could provide insight into the role of morphology, structure, and optical properties for the potential application of carbon dots in visible light-assisted photocatalytic applications.

Results and discussion

The nature of functional groups present in the as-synthesized N-CDs and S,N-CDs determines their optical properties that are evaluated by UV-Vis and photoluminescence spectroscopy. Fig. 1(a) shows the UV-Visible absorption spectra of the N-doped and S,N-doped carbon dots with different precursor weight ratios (citric acid : urea (C/U) and citric acid : thiourea (C/T)) synthesized at 250 °C. N-CD-1 features a prominent peak at $ca.$ 260 nm, which can be assigned to the $\pi \rightarrow \pi^*$ transition of C=C of the sp^2 domain. The higher urea/thiourea content results in a small peak around 330 nm due to the $n \rightarrow \pi^*$ transition. Also, a broadened shoulder at 410 nm has been observed with its tail extending in the entire visible region, which might be due to the presence of surface molecular centers. This becomes more evident with the decrease in the weight ratio of precursors.

To assess the emission induced by $\pi \rightarrow \pi^*$ and $n \rightarrow \pi^*$ absorption transitions, the photoluminescence spectra were analysed by varying the excitation wavelength from 280 to 600 nm. Photoluminescence emission follows Stokes' type emission; basically the photoluminescence emission wavelength is longer then the excitation wavelength. Also, the photoluminescence emission profile of different CDs in D.I. water shows the typical excitation wavelength-dependent behaviour by shifting the emission wavelength from 430 to 570 nm (Fig. S1, ESI†). For S,N-CDs, the emission peak maxima occurred at 370 and 430 nm corresponding to the excitation wavelengths of 340 nm for S,N-CD-1 and S,N-CD-2, respectively, which is due to the introduction of sulphur atoms. The excitation dependent emission characteristics are consistent with those of previously reported S,N-CDs (Fig. S1(c) and (d), ESI†).[24,25] Interestingly, the 3D photoluminescence spectra of the N-CD-1 and N-CD-2 have shown a red-shifted emission maxima at 530 nm along with 360 nm, (Fig. 1(b) and Fig. S2(b), ESI†). This red-shifted emission in the case of N-CDs is probably due to the interband transitions ($\pi^*-\pi$ type) as observed in previous reports based on solid-state synthesis.[20,26] With the increase in the nitrogen content in CDs at higher temperatures, a low-lying intermediate state occurs in between the band. This results in narrowing the energy gap and leads to red-shifted interstate transition at 530 nm. Another possible reason for the green emission is likely due to the presence of molecular fluorophores (HPPT) attached to carbon cores.[18,27]

HR-TEM analysis was carried out to identify the morphology, crystallinity, and size distribution. The TEM images indicate that the samples prepared with SPMA via the microwave method are well dispersed (Fig. 1(d) and Fig. S3, S4, ESI†) and the corresponding size distribution analysis in the histogram is shown in Fig. S3 and S4, ESI.† The value of the average nanoparticle size and polydispersity measurement was performed by Gaussian fitting of size distribution (see Table S1, ESI†).

The crystalline phase of the prepared CD samples was characterized using the powder XRD technique. All the samples show a characteristic peak at around 27° (2θ), corresponding to the $d_{(002)}$ reflection arising due to the interlayer stacking reflection.[4,18] Apart from this, the broad peak at around 13° (2θ) represents the $d_{(001)}$ reflection, indicating the amorphous characteristics which decreases with the increase in the urea/thiourea precursor ratio. Moreover, relatively higher intensity and sharper $d_{(002)}$ peaks have been observed for a higher amount of urea/thiourea precursor enriched carbon dots (N-CD-2, and S,N-CD-2) as compared to N-CD-1 and S,N-CD-1, respectively (Fig. 2).

Raman characterization is helpful in detecting the intrinsic properties of sp^2 carbon materials. The Raman spectra of all the carbon dots, as shown in Fig. S5 (ESI†), reveal the two usual peaks at around 1359 (D peak) and 1580 cm^{-1} (G peak). The peaks were observed with varying intensity values. Typically, the G band at 1580 cm^{-1} is a characteristic of crystallised graphitic carbon which illustrates the E_{2g} mode for graphite that signifies the vibration of sp^2 bonded C-atoms present in the lattice.[28,29] However, the presence of the D band at around 1360 cm^{-1} is evidence of amorphous characteristics, which corresponds to the vibration of C-atoms associated with dangling bonds in the termination plane of graphite with a disordered nature.[30]
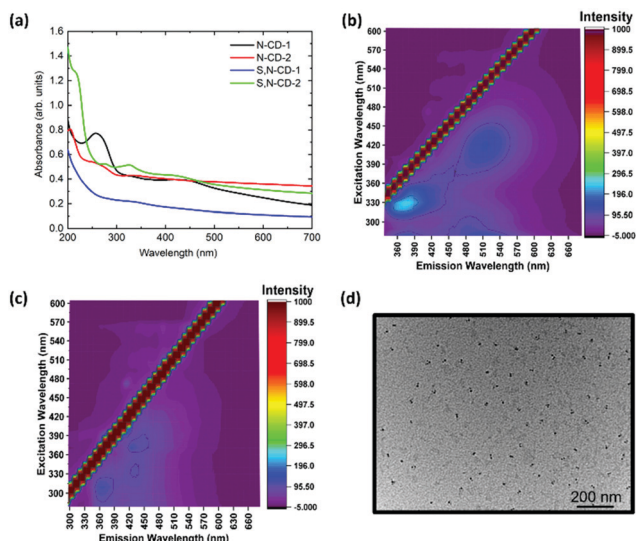

Fig. 1 (a) UV-visible absorption spectra of N-CD-1, N-CD-2, S,N-CD-1, and S,N-CD-2 in aqueous dispersion. 3-D photoluminescence spectra of (b) N-CD-2 and (c) S,N-CD-2. (d) HR-TEM images (scale bar = 200 nm) of N-CD-2.
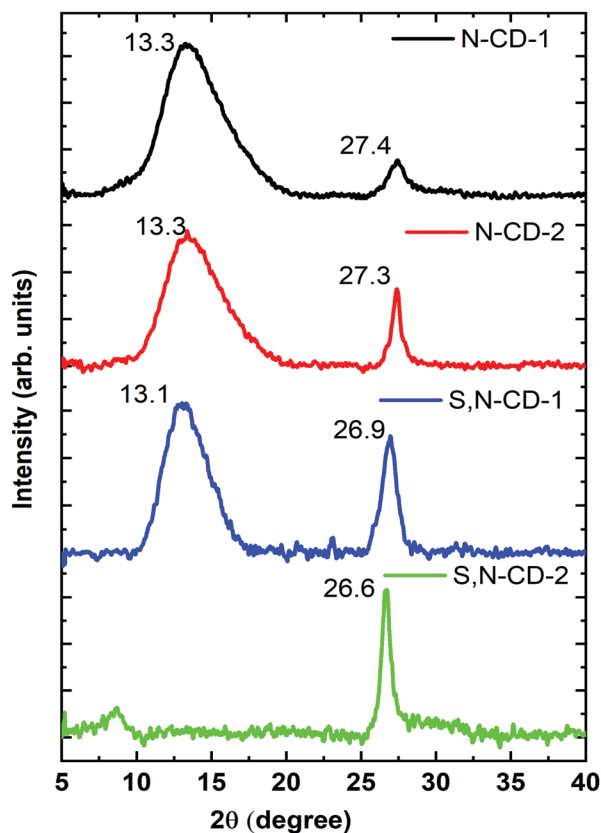
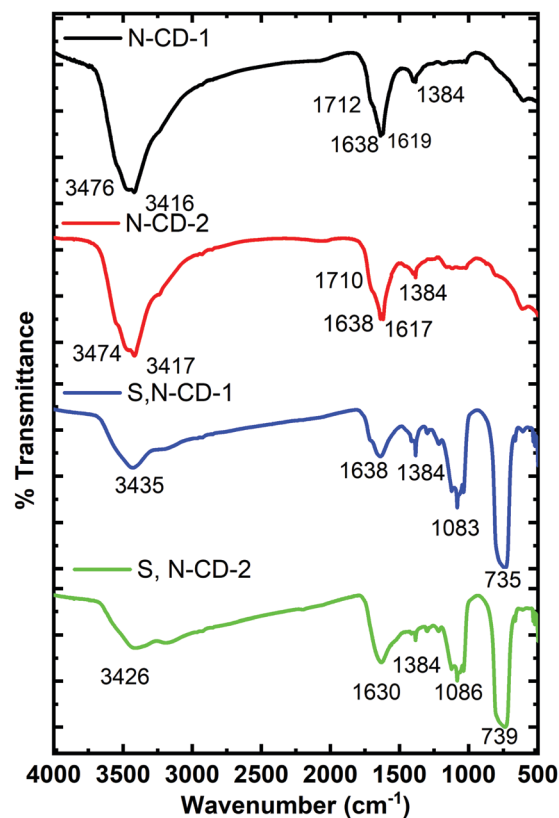Fig. 2 XRD spectra of N-CD-1, N-CD-2, S,N-CD-1, and S,N-CD-2.

Fig. 3 FTIR spectra of N-CD-1, N-CD-2, S,N-CD-1, and S,N-CD-2.

The FTIR Spectra of carbon dot samples were recorded to obtain the structural information (Fig. 3). The bands in the range of 3400 to 2900 cm^{-1} signify the presence of stretching vibrational modes of (O–H) and (N–H) functional groups. The peaks at ∼1710 and 1638 cm^{-1} are associated with the carbonyl and amide functional groups.[31] These peaks are stronger in N-CDs as compared to S,N-CDs signifying the presence of more amino functional groups. The signal at 1384 cm^{-1} is assigned to the stretching mode of C–N.[18,31] In S,N-CDs, the additional absorption features at 1080 and 735 cm^{-1} are ascribed to the stretching vibrations of C=S and C–S, respectively.[21]

Next, we turned to X-ray photoelectron spectroscopy (XPS) to investigate the elemental composition of carbon dots. In the full scan XPS spectrum of N-CD-2, as shown in Fig. 4(a), three characteristic peaks were found at 286.4, 400.6, and 532.4 eV, which correspond to C (1s), N (1s), and O (1s), respectively. On the other hand, two additional peaks, S (2s) – 229.7 eV and S (2p) – 164.7 eV, were observed for the S,N-CD sample, confirming the presence of sulfur atoms.[21] For N-CDs, the deconvoluted high-resolution spectrum of C (1s), Fig. 4(b), exhibits three characteristic peaks at 284.6 eV (sp^2 carbon, C=C), 285.7 eV (C–S or C–N), and 287.8 eV (C=O).[20,32] The relatively high intensity of the 284.6 eV peak indicates the presence of sp^2 enriched carbon atoms.[18] The peaks from the high-resolution spectra of O (1s) were observed at 531.1 eV and 532.2 eV confirming the formation of C=O and C–OH/ C–O–C bonds, respectively. This might be due to the presence

of atmospheric oxygen and from the solvent as well,[33,34] as shown in Fig. 4(c). The two peaks in the deconvoluted N (1s) high resolution spectra at 398.5 and 399.9 eV, as shown in Fig. 4(d), can be assigned to pyridinic and pyrrolic nitrogen, respectively.[35] Apart from this, for the S,N-CD sample, the deconvoluted spectra of S (2p) show five peaks at 161.6 eV for (S–H) bonds, 163.6 eV for (C–S$_n$–C, where, n = 1 or 2), representing a thiophene like structure, 164.9 eV for (–C=S– bonds), 168.0 eV for (–C–SO$_3$) bonds, and 169.2 eV representing the (–C–SO$_4$) bond formation in the prepared samples (see Fig. S6, ESI†).[36] The elemental composition analysis from the XPS spectra reveals that N-CD contains (33.8, 36.8, and 29.4)% carbon, oxygen, and nitrogen, respectively, while for the S,N-CD sample, the carbon, oxygen, and nitrogen contents are (29.4, 36.8, and 29.4)% respectively along with 30.9% sulfur.

Time-resolved photoluminescence of N-CDs and S,N-CDs was monitored using time-correlated single photon counting (TCSPC) to understand the excited state properties. The photoluminescence decay was monitored with pulsed excitation at 377 nm and the emission at 450 nm (see Fig. S7, ESI†). Photoluminescence decays of all the CDs demonstrate a biexponential decay (time constants are reported in the ESI,† Table S2). To this end, nitrogen doped carbon dots (N-CD-2) reveal the most extended lifetime with time constants of 2.94 and 10.06 ns. Interestingly, sulphur doped carbon dots (S,N-CDs) feature a slightly shorter lifetime.
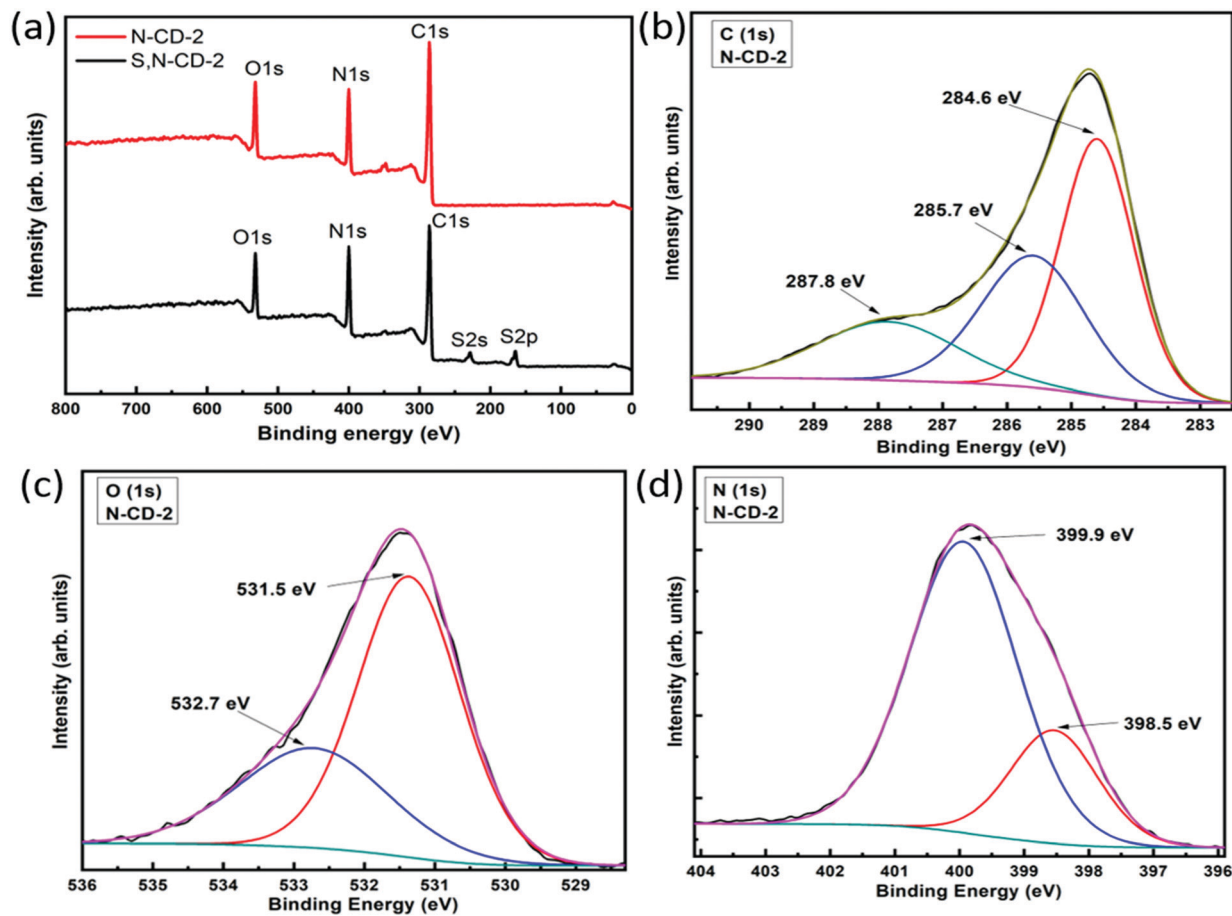
Fig. 4 (a) Survey-scan XPS spectra of N-CD and S,N-CD samples. High-resolution XPS spectra of the N-CD-2 sample: (b) C 1s, (c) O 1s, and (d) N 1s.

To understand the photoredox catalytic properties of N-CDs, and S,N-CDs, 410 and 455 nm wavelength LEDs were employed to study the conversion efficiency for the photoreduction of methyl viologen cations (MV^{2+}, -0.45 V $vs.$ NHE) in the presence of EDTA as a sacrificial hole scavenger (see Fig. S8 and S9, ESI†). The photoreduction of methyl viologen to form a blue color radical cation has been extensively studied to understand the electron transfer properties of different nanomaterials, including carbon dots.[23,37–39] Positively charged MV^{2+} are likely to be attached onto the surface of negatively charged carbon dots through electrostatic interaction, which facilitates the electron transfer from CDs to MV^{2+} under photoexcitation.[40] Conversion of MV^{2+} to $MV^{•+}$ is a reversible process indicated by the colour change from colorless to blue, which is monitored by the presence of a 605 nm peak in the UV-Vis absorption spectra. In this case, the zeta potential values of all the samples are in the range of -34.3 to -17.96 mV (see Table S3 and Fig. S10, ESI†). Among all the CDs, N-CD-2 demonstrates the highest conversion ($\sim$3.5%) and ($\sim$7.0%) efficiency on illumination with 455 nm and 410 nm LEDs, respectively, as shown in Fig. 5(a) and (b), respectively. It should be noted that although previous reports on carbon dot-based photoreduction of methyl viologen have shown higher efficiency, they have employed high-intensity UV-LEDs (365 nm) or solar simulators

as light sources.[22,23] The overall trends for the conversion efficiency was observed as (N-CD-2 > S,N-CD-2 > S,N-CD-1 > N-CD-1) for the 410 nm LED and (N-CD-2 > S,N-CD-2 > N-CD-1 > S,N-CD-1) for the 455 nm LED. This illustrates that the presence of nitrogen plays a more important role than sulfur for the photoinduced electron properties of carbon dots. Also, a higher conversion efficiency was observed in the case of a 410 nm LED as compared to the illumination with a 455 nm LED because of the higher absorption of all the prepared CDs in the near visible region as observed from the UV-Vis absorption spectra, – Fig. 1(a). The higher conversion efficiency can be explained by the long photoluminescence lifetime of N-CD-2. Furthermore, recent ultrafast spectroscopic studies have demonstrated that back electron transfer between the photoexcited holes in carbon dots and methyl viologen radical cations is slower in N-doped carbon dots in comparison with other heteroatom doped carbon dots.[41]

The photoredox catalytic nature of N-CD-2 was further investigated by monitoring the kinetics of $MV^{•+}$ formation through sequential photoinduced electron transfers.[22] After 1 h of illumination for each set of photoreduction, the resultant blue solution was allowed to become colorless overnight. A similar rate of formation of $MV^{•+}$ was observed for subsequent runs (runs 2 and 3), indicating the reversibility of the electron
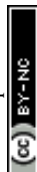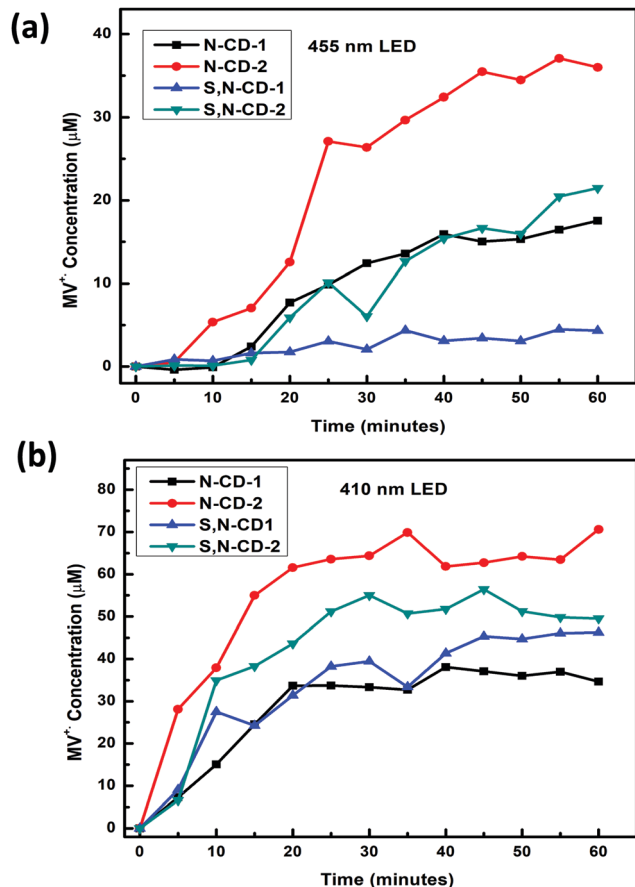
Fig. 5 (a) Kinetics of MV$^{\bullet+}$ formation for all samples under 455 nm illumination. (b) Kinetics of MV$^{\bullet+}$ formation for all samples under 410 nm illumination.

transfer process, as shown in Fig. S11 and S12 (ESI†) for 410 nm and 455 nm LEDs, respectively.

Conclusions

In this work, solid-state microwave synthesis of heteroatom-doped carbon dots is demonstrated. The photoredox properties of doped carbon dots were studied by investigating the model photoreduction of methyl viologen. The graphitic nature of the carbon dots was more prominent in urea/thiourea precursor enriched carbon dots. To this end, nitrogen-doped carbon dots with a higher urea precursor content demonstrate the highest photoconversion efficiency of methyl viologen in the presence of 410 and 455 nm wavelength LEDs. The results herein reported show that nitrogen-doped carbon dots are better electron transfer agents than sulfur, nitrogen-co-doped carbon dots under visible light irradiation.

Materials and methods

Chemicals

Citric acid (Sigma-Aldrich, ≥99.5%), urea (TCI Chemicals, >99%), thiourea (Sisco Research Laboratories Pvt. Ltd AR, 99%),

EDTA (Loba Chemie Laboratory Reagents and Fine Chemicals, 99%) and methyl viologen dichloride hydrate (Aldrich, 98%) were used as purchased and without further modification.

Synthesis of CDs

Carbon dots were synthesized using the solid-state microwave bottom-up synthesis approach. Briefly, 0.5 g of citric acid and 0.5 g of urea were mixed uniformly with a mortar and pestle. The weight ratio of citric acid and urea was varied for N-CD-1 and N-CD-2. 0.5 g of the resultant mixture was taken in a glass microwave vial with an inner volume of 30 mL and sealed with a PTFE-lined cap. The mixture was heated at 250 °C for 10 min with a microwave reactor (Anton-Paar, Monowave 200). During the process of microwave heating, stirring was done with a magnetic stir bar present in the reaction mixture at 600 rpm. After 10 minutes of reaction, the system was cooled down to 55 °C. The inner temperature and pressure conditions were managed and maintained through an internal IR thermometer and pressure sensor, respectively. Then, the product was extracted from the vial and dissolved in D.I. water to form a homogeneous aqueous dispersion using an ultra-sonication process and purification was performed *via* dialysis using Spectra/MWCO: 500–1000 D for three consecutive days. Followed by dialysis, the final product was obtained by the freeze–drying process. The same procedure was employed for the synthesis of S,N-CDs samples by replacing urea with thiourea as a source of nitrogen and sulfur. All the samples are denoted by their doped atoms; nitrogen doped carbon dots and nitrogen and sulphur co-doped carbon dots with weight ratios (1:1 and 1:3) are denoted as N-CD-1, N-CD-2, S,N-CD-1 and S,N-CD-2, respectively.

Characterization

The UV/Vis spectra of the aqueous dispersion of CDs were obtained using a Cary 4000 UV-Vis double beam spectrophotometer. The crystalline nature of the CDs was characterized with a Model D8 Advance, Bruker AXS X-ray diffractometer using Cu Kα radiation. The Fourier transform infrared spectra were obtained using a Nicolet iS10 FTIR spectrophotometer using IR grade KBr powder. The photoluminescence spectra of the aqueous dispersion of CDs were recorded with a Cary Eclipse fluorescence spectrophotometer. High-resolution transmission electron microscopy images were recorded on a 200 kV JEM-2100 transmission electron microscope. The samples were prepared by drop-casting onto a carbon-coated copper grid, followed by drying at room temperature. X-Ray photoelectron spectroscopy (XPS) analysis was performed with a Thermo Scientific XPS, Model MULTILAB 2000 base system, having twin anodes Mg/Al (300–400 W) and an X-ray source electron gun having a spot size of <50 mm diameter. PL lifetime decays of an aqueous dispersion of carbon dots were monitored using 377 nm picosecond pulsed diode laser (5 mW) excitation and time-resolved spectrophotometer (Edinburgh Instruments, FLS920). The zeta potential of the carbon dots was measured in aqueous solution using a Zetasizer NanoZS instrument (Malvern, UK).

Photo-redox catalytic studies

The photo-redox properties of carbon dots were studied by performing photo-reduction experiments of methyl viologen to $MV^{\bullet+}$ radicals, using 410 nm and 455 nm LEDs (Holmarc Opto-Mechatronics Pvt. Ltd, Model-HO-HBL-3M). Briefly, 50 μg mL^{-1} of an aqueous solution of CDs were prepared in ethylene diamine tetracetic acid (EDTA, 0.1 M, pH 6) with the addition of MV^{2+} (1 mM). Then, ~3 mL of the solution was irradiated with a visible light-emitting diode lamp (LED, wavelength = 455 nm, irradiance of 33 mW cm^{-2} and wavelength = 410 nm, irradiance of 26 mW cm^{-2}), after purging with argon gas for 10 minutes. Furthermore, the generation of $MV^{\bullet+}$ radical cations was monitored (for 60 min) by the emergence of a new peak around 605 nm (ε = 13 700 M^{-1} cm^{-1}) using a UV-visible spectrophotometer. The monochromatic nature of LED light sources was supported by absorption spectra taken via an absorption spectrometer (Avantes Starline, Avaspec-3648) (Fig. S13 and S14) (ESI†).

Author contributions

The manuscript was written through the contributions from all authors. All authors have approved the final version of the manuscript.

Conflicts of interest

There are no conflicts to declare.

Acknowledgements

Notes and references

1 X. Xu, R. Ray, Y. Gu, H. J. Ploehn, L. Gearheart, K. Raker and W. A. Scrivens, *J. Am. Chem. Soc.*, 2004, **126**, 12736–12737.

2 J. Jiang, G. Ye, Z. Wang, Y. Lu, J. Chen and K. Matyjaszewski, *Angew. Chem., Int. Ed.*, 2018, **57**, 12037–12042.

3 S. Cailotto, M. Negrato, S. Daniele, R. Luque, M. Selva, E. Amadio and A. Perosa, *Green Chem.*, 2020, **22**, 1145–1149.

4 B. C. M. Martindale, G. A. M. Hutton, C. A. Caputo, S. Prantl, R. Godin, J. R. Durrant and E. Reisner, *Angew. Chem., Int. Ed.*, 2017, **56**, 6459–6463.

5 X. Qie, M. Zan, P. Miao, L. Li, Z. Chang, M. Ge, P. Gui, Y. Tang and W.-F. Dong, *J. Mater. Chem. B*, 2018, **6**, 3549–3554.

6 Q. Zhu, L. Zhang, K. Van Vliet, A. Miserez and N. Holten-Andersen, *ACS Appl. Mater. Interfaces*, 2018, **10**, 10409–10418.

7 F. F. Du, Z. H. Guo, Z. Cheng, M. Kremer, S. M. Shuang, Y. Liu and C. Dong, *Nanoscale*, 2020, **12**, 20482–20490.

8 T. Guerrero-Esteban, C. Gutiérrez-Sánchez, E. Martínez-Periñán, M. Revenga-Parra, F. Pariente and E. Lorenzo, *Sens. Actuators, B*, 2021, **330**, 129389.

9 L. J. Zhang, Y. M. Yang, M. A. Ziaee, K. L. Lu and R. H. Wang, *ACS Appl. Mater. Interfaces*, 2018, **10**, 9460–9467.

10 Z. T. Zhang, G. Y. Yi, P. Li, X. X. Zhang, H. Y. Fan, Y. L. Zhang, X. D. Wang and C. X. Zhang, *Nanoscale*, 2020, **12**, 13899–13906.

11 T.-N. Pham-Truong, C. Ranjan, H. Randriamahazaka and J. Ghilane, *Catal. Today*, 2019, **335**, 381–387.

12 D. H. Hasenöhrl, A. Saha, V. Strauss, L. Wibmer, S. Klein, D. M. Guldi and A. Hirsch, *J. Mater. Chem. B*, 2017, **5**, 8591–8599.

13 F. H. Horst, C. V. D. Rodrigues, P. Carvalho, A. M. Leite, R. B. Azevedo, B. A. D. Neto, J. R. Correa, M. P. Garcia, S. Alotaibi, M. Henini, S. B. Chaves and M. O. Rodrigues, *RSC Adv.*, 2021, **11**, 6346–6352.

14 B. B. Karakocak, A. Laradji, T. Primeau, M. Y. Berezin, S. Q. Li and N. Ravi, *ACS Appl. Mater. Interfaces*, 2021, **13**, 277–286.

15 Y.-Y. Chen, W.-P. Jiang, H.-L. Chen, H.-C. Huang, G.-J. Huang, H.-M. Chiang, C.-C. Chang, C.-L. Huang and T.-Y. Juang, *RSC Adv.*, 2021, **11**, 16661–16674.

16 J. Schneider, C. J. Reckmeier, Y. Xiong, M. von Seckendorff, A. S. Susha, P. Kasák and A. L. Rogach, *J. Phys. Chem. C*, 2017, **121**, 2014–2022.

17 W. Kasprzyk, T. Świergosz, S. Bednarz, K. Walas, N. V. Bashmakova and D. Bogdał, *Nanoscale*, 2018, **10**, 13889–13894.

18 V. Strauss, H. Wang, S. Delacroix, M. Ledendecker and P. Wessig, *Chem. Sci.*, 2020, **11**, 8256–8266.

19 N. M. Zholobak, A. L. Popov, A. B. Shcherbakov, N. R. Popova, M. M. Guzyk, V. P. Antonovich, A. V. Yegorova, Y. V. Scrypynets, I. I. Leonenko, A. Y. Baranchikov and V. K. Ivanov, *Beilstein J. Nanotechnol.*, 2016, **7**, 1905–1917.

20 S. Gu, C.-T. Hsieh, Y. Ashraf Gandomi, J.-K. Chang, J. Li, J. Li, H. Zhang, Q. Guo, K. C. Lau and R. Pandey, *J. Mater. Chem. C*, 2019, **7**, 5468–5476.

21 D. Qu, M. Zheng, P. Du, Y. Zhou, L. Zhang, D. Li, H. Tan, Z. Zhao, Z. Xie and Z. Sun, *Nanoscale*, 2013, **5**, 12272–12277.

22 S. Cailotto, R. Mazzaro, F. Enrichi, A. Vomiero, M. Selva, E. Cattaruzza, D. Cristofori, E. Amadio and A. Perosa, *ACS Appl. Mater. Interfaces*, 2018, **10**, 40560–40567.

23 F. Rigodanza, L. Đorđević, F. Arcudi and M. Prato, *Angew. Chem., Int. Ed.*, 2018, **57**, 5062–5067.

24 Y. Dong, H. Pang, H. B. Yang, C. Guo, J. Shao, Y. Chi, C. M. Li and T. Yu, *Angew. Chem.*, 2013, **52**, 7800–7804.

25 T. Liu, Z.-W. Cui, J. Zhou, Y. Wang and Z.-G. Zou, *Nanoscale Res. Lett.*, 2017, **12**, 375.

26 S. Gu, C.-T. Hsieh, Y. Ashraf Gandomi, J. Li, X. X. Yue and J.-K. Chang, *Nanoscale*, 2019, **11**, 16553–16561.

27 J. D. Stachowska, A. Murphy, C. Mellor, D. Fernandes, E. N. Gibbons, M. J. Krysmann, A. Kelarakis, E. Burgaz, J. Moore and S. G. Yeates, *Sci. Rep.*, 2021, **11**, 10554.

28 M. Righetto, A. Privitera, I. Fortunati, D. Mosconi, M. Zerbetto, M. L. Curri, M. Corricelli, A. Moretto, S. Agnoli, L. Franco, R. Bozio and C. Ferrante, *J. Phys. Chem. Lett.*, 2017, **8**, 2236–2242.

29 K. J. Mintz, Y. Zhou and R. M. Leblanc, *Nanoscale*, 2019, **11**, 4634–4652.

30 H. Li, X. He, Z. Kang, H. Huang, Y. Liu, J. Liu, S. Lian, C. H. A. Tsang, X. Yang and S.-T. Lee, *Angew. Chem.*, 2010, **49**, 4430–4434.

31 Z. S. Schroer, Y. Wu, Y. Xing, X. Wu, X. Liu, X. Wang, O. G. Pino, C. Zhou, C. Combs, Q. Pu, M. Wu, J. X. Zhao and J. Chen, *ACS Appl. Nano Mater.*, 2019, **2**, 6858–6865.

32 M. Meng, H. Yan, Y. Jiao, A. Wu, X. Zhang, R. Wang and C. Tian, *RSC Adv.*, 2016, **6**, 29303–29307.

33 Y.-C. Lu, J. Chen, A.-J. Wang, N. Bao, J.-J. Feng, W. Wang and L. Shao, *J. Mater. Chem. C*, 2015, **3**, 73–78.

34 Z. Qian, J. Ma, X. Shan, H. Feng, L. Shao and J. Chen, *Chem. – Eur. J.*, 2014, **20**, 2254–2263.

35 T. Kondo, S. Casolo, T. Suzuki, T. Shikano, M. Sakurai, Y. Harada, M. Saito, M. Oshima, M. I. Trioni, G. F. Tantardini and J. Nakamura, *Phys. Rev. B: Condens. Matter Mater. Phys.*, 2012, **86**, 035436.

36 C. Shen, S. Ge, Y. Pang, F. Xi, J. Liu, X. Dong and P. Chen, *J. Mater. Chem. B*, 2017, **5**, 6593–6600.

37 F. Zhao, Q. Li, K. Han and T. Lian, *J. Phys. Chem. C*, 2018, **122**, 17136–17142.

38 A. Saha, A. Moya, A. Kahnt, D. Iglesias, S. Marchesan, R. Wannemacher, M. Prato, J. J. Vilatela and D. M. Guldi, *Nanoscale*, 2017, **9**, 7911–7921.

39 G. T. Brown and J. R. Darwent, *J. Chem. Soc., Faraday Trans.*, 1984, **80**, 1631–1643.

40 V. Strauss, J. T. Margraf, C. Dolle, B. Butz, T. J. Nacken, J. Walter, W. Bauer, W. Peukert, E. Spiecker, T. Clark and D. M. Guldi, *J. Am. Chem. Soc.*, 2014, **136**, 17308–17316.

41 S. Mondal, A. Yucknovsky, K. Akulov, N. Ghorai, T. Schwartz, H. N. Ghosh and N. Amdursky, *J. Am. Chem. Soc.*, 2019, **141**, 15413–15422.